ORIGINAL ARTICLE

Effect of metallurgical parameters on the drilling and tapping characteristics of aluminum cast alloys

H. Barakat [1] · Y. Zedan [2] · A. M. Samuel [1] · H. W. Doty [3] · S. Valtierra [4] · F. H. Samuel [1]

Abstract
The present study was performed on an Al-6% Cu-0.7%Si alloy, and 319 and 356 alloys following different heat treatments. The main task was to evaluate the drilling and tapping characteristics of the Al-Cu alloy with respect to the Al-Si-based 319 and 356 alloys. The drilling work was carried out on a Huron K2X8five CNC machine at 15,000 rpm with continuous cooling to absorb the heat and to clean the holes from the chips formed during the drilling operation. The results show that the addition of Si coupled with T6 aging treatment produces the highest cutting forces (about 360 N) among the alloys studied (approximately 270 N) after 2500 holes. Considering the Al-Cu-based alloys, varying the aging treatment has practically no significant bearing on the cutting forces. Apparently, a high Cu content acts as a self-lubricant, facilitating the drilling process up to 2700 holes, with no sign of tool wear. However, due to the low level of Si in the Al-Cu-based alloy, built up edge (BUE) is more frequent, with conical chips, which would affect the precision of the size of the drilled hole. The chips are normally dull and characterized by their rough surfaces compared to those obtained from A356.0 alloy. Tapping of the drilled holes was carried out using Guhring 971 H6 M6 6HX- HSSE taps. The HT200-based alloys revealed excellent machinability with no sign of tool wearing after 2500 holes. In contrast, the tool failed after 1600 holes in the case of 356 alloy and 2160 holes for 319 alloy. Thus, it is concluded that the presence of 3.5% Cu in the 319 alloy helped in reducing the severity of wearing due to eutectic Si particles. However, the tapping forces reached 120 N prior to failure compared to about 75 N in the case of T200-based alloys.

Keywords Al-Cu alloys · Drilling · Tapping · BUE · Cutting forces · Tool wearing

1 Introduction

Considering machinability as a system property allows us to define machinability as an interaction phenomenon between the workpiece, cutting tool (tool material and geometry), and cutting medium (wet or dry cutting) for different removal sequences such as turning, drilling, tapping, milling, and sawing under different cutting conditions which are cutting speed, feed rate, and depth of

cut [1–6]. Many research investigations were undertaken in order to analyze the role of the tool geometry on the machinability of different alloys under different cutting conditions for different machining processes. In the case of turning, Fang et al. [7] introduced a new model to predict chip formation in chamfered and honed tools for aluminum alloys and concluded that the ratio between thrust force and cutting force varies according to the thickness of the uncut chip. In addition, the thrust force can exceed the cutting force if the uncut chip thickness is less than the critical thickness, which can be determined by the cutting speed and tool geometry [8–10]. On the other hand, with respect to drilling, Tash [9] reported that in casting alloys with highly abrasive materials, it is preferable to use solid carbide drills with twist drills to make the edges more resistant to wear at higher speeds [10, 11]. Soares et al. [12] investigated chip breaker systems in different cemented carbide and PCD diamond cutting tools, in order to evaluate their quality in the machining of aluminum alloys. They

✉ F. H. Samuel
   fhsamuel@uqac.ca

1 Département des Sciences appliquées, Université du Québec à Chicoutimi, Chicoutimi, QC, Canada

2 Département de génie mécanique, École de technologie supérieure, Montreal, QC, Canada

3 General Motors Materials Engineering, 823 Joslyn Ave, Pontiac, MI 48340, USA

4 Nemak, S.A., P.O. Box 100, 66221 Garza Garcia, N.L., Mexico

Fig. 1 Schematic diagram illustrating the machining environment [16]
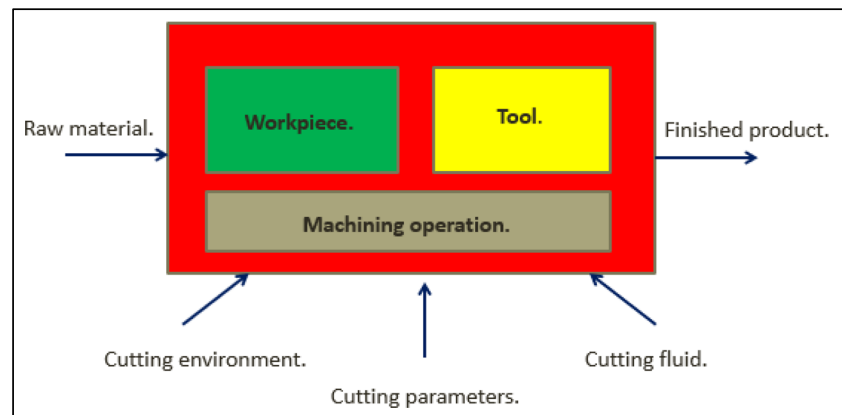
reported that inserts with big grooves, and a high angle of entrance in the chip breaker, showed good results in power consumption, surface roughness, and chip control for roughing operations ($f > 0.14$ mm/rev) in high silicon-containing aluminum alloys [13].

Tool wear is the main factor that controls tool life. It takes place as a gradual process because of continuous interaction between the cutting edge and workpiece under specific cutting conditions, until the failure of the tool. The wear process depends on tool material and geometry, workpiece material, and the cutting parameters and medium [12, 14]. Material properties such as strength, ductility, and hardness also affect different machinability aspects as cutting force, chip formation, and surface integrity [15]. Hamed [16] has summarized the above findings schematically as shown in Fig. 1.

The present work was undertaken to optimize the alloy composition and heat treatment conditions, and to compare its performance with the widely used Al-Si based 319 and 356 commercial alloys [17]. The study was extended to also investigate the machinability behavior of the HT200 alloy castings under the different heat treatment conditions, to include this important aspect of the production process. This article presents the results on drilling and tapping of HT200 alloy castings and compares them with those of the 319 and 356 reference alloys. It should be mentioned here that the drilling and tapping parameters using a CNC machining center were decided in consultation with senior designing engineers from General Motors–USA.

2 Experimental procedure

The HT200 base alloy was supplied by Nemak. The composition of the alloy shown in Table 1 is proprietary to Nemak. The alloy is an Al-Cu alloy containing higher Si than 206 and 201 alloys, but a much lower concentration of silicon in comparison to the Al-Si-based B319 and A356 alloys which were used as reference alloys for comparison with the HT200 alloys. The 319 and 356 alloys were grain refined and modified using Al-5%Ti-1%B and Al-10%Sr master alloys, respectively. In the context of these alloys, it is important to mention here that in a previous study carried out by Zedan [15], the effect of metallurgical parameters on the machining behavior (drilling and tapping) of 356 and 319 alloys was studied using a Makino A88E machine for which extensive machinability data was collected. In the present case, a Huron K2X8five CNC machine was employed and the same 319 and 356 alloys were used to confirm the data obtained. It is in this sense, therefore, that these alloys are considered as reference alloys for comparison purposes with the HT200 alloy in the present study.

A nomination system was used to identify the alloys. Alloy A was used to indicate HT200 alloy in the as-cast condition, alloy B was used to identify HT200 alloy subjected to T5 heat treatment, while alloy C was used to indicate HT200 alloy subjected to T7 heat treatment, and the reference alloys B319 and A356 were termed alloy D and alloy E, respectively. The alloys used in this study were provided in the form of ingots, cut into smaller pieces, dried and melted in a SiC crucible of 120-kg capacity at a temperature of $750° \pm 5$ °C,

Table 1 Chemical analysis of the studied alloys

Alloy	Chemical analysis (wt%)										
	Elements										
	Cu	Si	Fe	Mn	Mg	Ti	Zr	V	Zn	Sr	Al
HT200	6.0	0.69	0.17	0.38	0.02	0.10	0.19	0.013	0.19	–	Bal
B319.1	3.09	5.66	1.06	0.39	0.27	0.13				0.0180	Bal
A356.1	0.12	7.19	0.12	–	0.32	0.12	–	–		0.0165	Bal

Fig. 2 **a** Mold used for preparing castings for drilling tests, **b** casting obtained

(a)   (b)
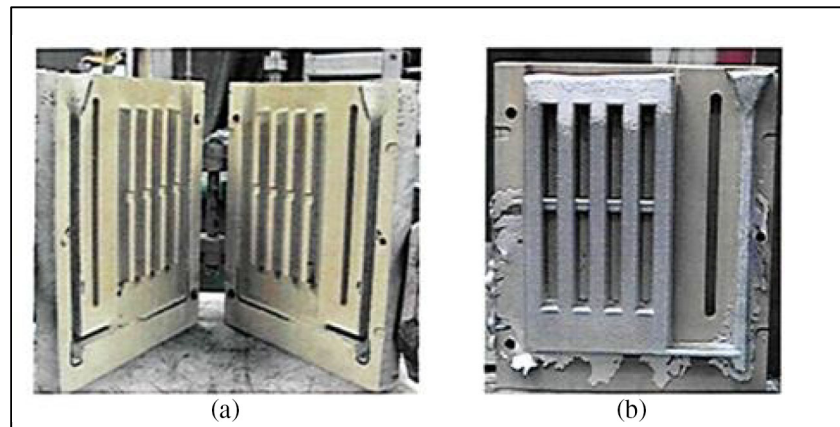
using an electric resistance furnace. Measured amounts of additives were calculated and added to the melt using a perforated graphite bell, plunged deep into the melt to ensure homogeneous distribution.

The melt was degassed by injecting dry argon gas into the melt at a constant rate for 15–20 min by means of a degassing impeller rotating at a speed 120–130 rpm. Following degassing, the melt surface was carefully skimmed to remove the dross and oxide inclusions. Then, the melt was poured at 740 °C into the waffle-plate graphite-coated metallic mold shown in Fig. 2 to produce the castings for conducting the drilling tests, and an ASTM B-108 permanent mold for preparing tensile test bars. The machinability test casting blocks had initial dimensions of 300-mm length, 200-mm width, and 30-mm thickness with five ribs with an average width of 25.4 mm. Seventy castings were produced for the drilling tests. A summary of the heat treatments used is presented in Table 2. It should be mentioned here that heat treatment of Al-Cu alloys was recommended by Nemak-Europe whereas heat treatment of 319 and 356 alloys were based on the authors 30 years of experience.

Tensile test bars (5 bars per alloy in the form of a bundle) from the different alloys were prepared using the ASTM B-108 mold, and heat treated following the same procedures as in the case of the blocks. Each bundle consists of five test bars with standard dimensions (50-mm length and 12.7-mm cross-sectional diameter) in order to evaluate the average tensile properties (UTS, YS, and %El) over the five bars tested in each case. The tests were carried out at ambient temperature (25 °C). A Servohydraulic MTS Mechanical Testing machine was used to carry out the tests, using a strain rate of 4×10^{-4} s^{-1}. A strain gauge extensometer (with a 50.8-mm range) attached to the gauge length of the test bar was used to measure the elongation. The data was recorded by the data acquisition system of the machine and analyzed using the Test Works 4 software associated with the system to provide the yield strength at 0.2% offset strain, ultimate tensile strength, and the percentage elongation values.

The drilling process was carried out at a cutting speed of 240 m/min (15,000 rpm) and 0.2 mm/rev feed rate, using a Guhring 16101256 M6 drilling tool from Carbide steel, as shown in Fig. 3. The coolant used while drilling was Hocut 4549, normally used with high-speed processes. The machining conditions are summarized in Table 3. Prior to drilling, the machine was calibrated by the specialist from the Aeronautical Technology Center where the work took place.

The drilling characteristics of the HT200 and reference alloys were evaluated by means of cutting force measurements, tool life evaluation, built up edge (BUE) measurements, and chip formation characteristics. Tapping of the drilled holes was carried out using Guhring 971 H6 M6 6HX-Carbide taps (Fig. 3b). These tap series are classified

Table 2 Heat treatment procedure

Alloy code	Alloy type	Heat treatment					
		Working condition	SHT* temperature	Time	Aging temperature	Time**
A	HT200	As-cast	–	–	–	–
B	HT200	T5	–	–	250 °C	4 h
C	HT200	T7	520 °C	8 h	250 °C	4 h
D	B319.0	T7	510 °C	8 h	250 °C	4 h
E	A356.0	T6	540 °C	8 h	180 °C	4 h

*Samples were quenched in warm water (60 °C) after SHT. **Samples were air-cooled after aging
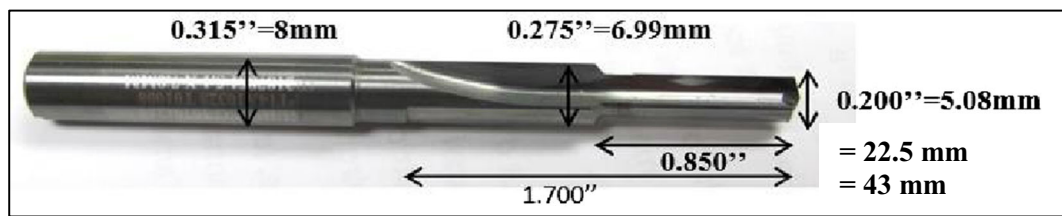
a   Shape and dimensions of the used drilling tool.
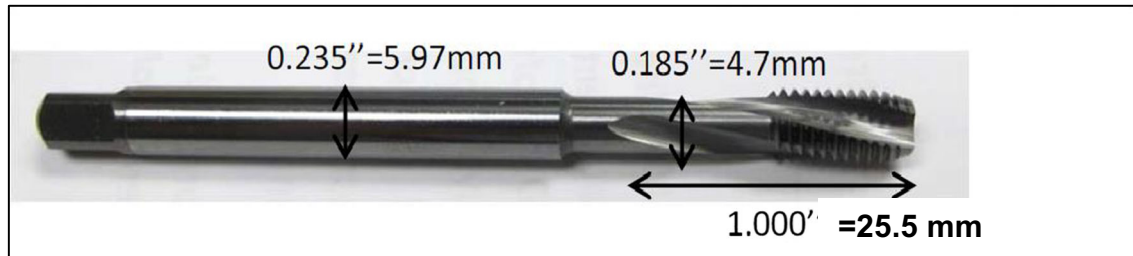
b   Shape and dimensions of the tapping tool used in the present work.

Fig. 3 a Shape and dimensions of the used drilling tool. **b** Shape and dimensions of the tapping tool used in the present work

as carbide tools, with a significant concentration of cobalt. This concentration enhances the wear resistance of the carbide taps and, more importantly, results in a longer than average tool life.

For determining the cutting forces, a specific configuration was employed to carry out the test, in which four 6-component piezoelectric quartz crystal dynamometers were installed on the base plate which accommodated the workpiece. These dynamometers transform the acting forces into proportional electric charges, which can then be transformed in terms of newton according to the charge intensity. Eight charges are generated by these four dynamometers in different directions, which are Fx_{12}, Fx_{34}, Fy_{14}, Fy_{23}, Fz_1, Fz_2, Fz_3, Fz_4, at a sampling rate of 10 MHz, which means that eight readings are recorded every 0.0000001 s during the whole machining process. Charge conversion into forces takes place by passing the charges through amplifiers in order to magnify the signal, then converting them by analog to digital circuit, then representing the data and recording it through a special interface on LabView. The data is then used to calculate the major force components and moment components.

A specific plan was followed to evaluate built up edge and tool wear, by measuring these periodically after drilling a certain number of holes for the five alloys. A Keyence 2000 type digital microscope with × 100 magnification was used to facilitate clear examination and measurement of the wear and built up accumulation. In addition to tool wear and built up edge evaluation, a chip characterization test was also done by measuring the

Table 3 Machining conditions for drilling

Machine	Huron K2X8 machine
Coolant	Hocut 4549
Drilling	
Drilling tool	Guhring 16101256, PT14A 10328, T01008, ID2187851 5.1 × 7.0 mm
Drilling speed	240 m/min
Feed rate	0.2 mm/rev
Diameter	M6 standard hole
Depth	22.5 mm ± 0.5
Tapping	
Tapping tool	Guhring 971 H6 M6 6HX, HM K/P 15.0/70.3, 33442
Drilling speed	45 m/min
Feed rate	By pitch
Depth	18 mm ± 0.5
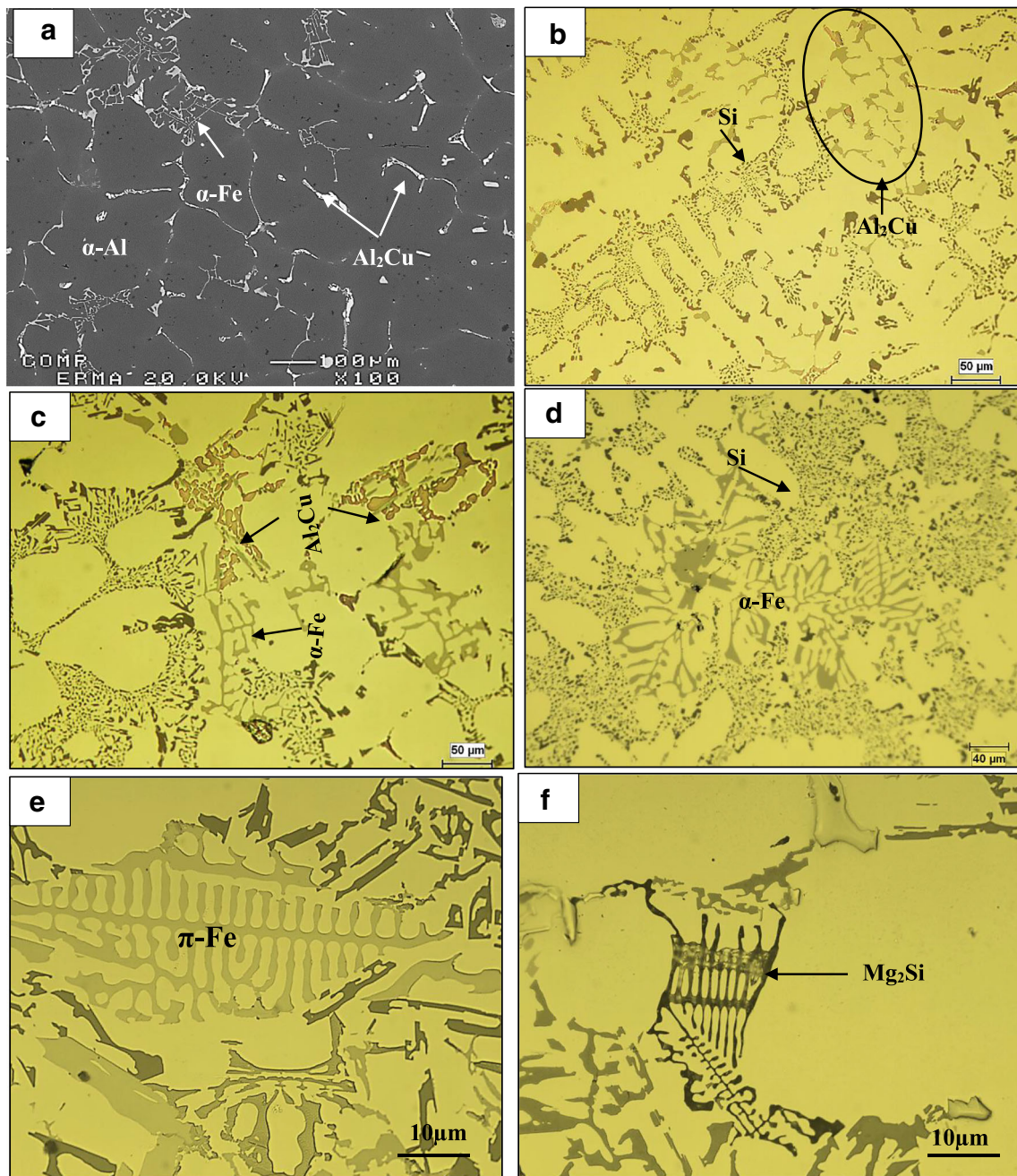
Fig. 4 Microstructure of as-cast: **a** alloy A; **b**, **c** alloy D; **d**–**f** alloy E

Table 4 Tensile properties of the studied alloys

Alloy	UTS (MPa)	YS (MPa)	EL%
Alloy A	283 ± 7	212 ± 5	2.2 ± 0.3
Alloy B	298 ± 9	235 ± 6	3.4 ± 0.4
Alloy C	331 ± 8	247 ± 5	5.3 ± 0.3
Alloy D	295 ± 10	244 ± 8	3.8 ± 0.2
Alloy E	355 ± 9	310 ± 6	6.9 ± 0.3

number of chips obtained for a specific mass of removed material for the five alloys, using a calibrated weight scale.

The data collected from the drilling process were imported in the form of mdt files to be processed on MATLAB. A sophisticated code was written in order to read, represent, and process the data with the aid of specialized libraries such as signal process toolbox and curve fitting library. The raw data were the forces recorded between every two sensors for the horizontal forces, and the recorded values from each sensor in vertical forces, in a high frequency rate of recording (10 MHz).

3 Results and discussion

3.1 Microstructure and tensile properties

Figure 4 shows the optical microstructures of the three alloys—A, D, and E—sectioned from their as-cast tensile bars. The large amount of Cu in the alloy A reflected in the precipitation of coarse Al_2Cu phase throughout the entire matrix along with a few α-$Al_{15}(Fe,Mn)_3Si_2$ phase particles as presented in Fig. 4a. As reported earlier [18], modification with Sr would lead to a divorced eutectic reaction where (Al-Si) eutectic has been observed separated from the (Al-Al_2Cu) one-alloy D (Fig. 4b). In addition, the α-Fe phase particles are also rejected in front of the advancing (Al-Si) eutectic (Fig. 4c). Pucella et al. [14] reported on the inverse precipitation of α-Fe in Sr-modified alloys. In this case, the α-Fe phase precipitates within the α-Al during solidification of the alloy (Fig. 4d). In other words, the α-Fe precipitates prior to the formation of the α-Al network. The importance of this reaction is to harden the soft α-Al leading to more-or-less uniform strength over the entire alloy. Figure 4e is an enlarged micrograph of alloy E revealing partial transformation of β-Al_5FeSi phase to π-Al_8Mg_3FeSi phase at ~ 560 °C followed by the precipitation of Mg_2Si phase at about 545 °C (Fig. 4f) [19].

Table 4 lists the tensile properties of the five used alloys following the heat treatments described in Table 2. The as-cast HT200 alloy itself shows relatively good characteristics, with almost 96% of the yield strength of the 319 alloy after T7 treatment, but with a significantly low ultimate tensile strength and elongation.

The T5 heat treatment of alloy B for 5 h increased its elongation by 1.2%, coupled with a slight improvement in its ultimate tensile strength by about 5% and better improvement in the alloy yield strength by about 12%, from the original as-cast value (alloy A). In comparison, alloy C (in the T7-treated condition) showed real improvement in all three properties: the elongation increased by about 3% and both the yield strength and the ultimate tensile strength increased by about 17% above those obtained from alloy A.
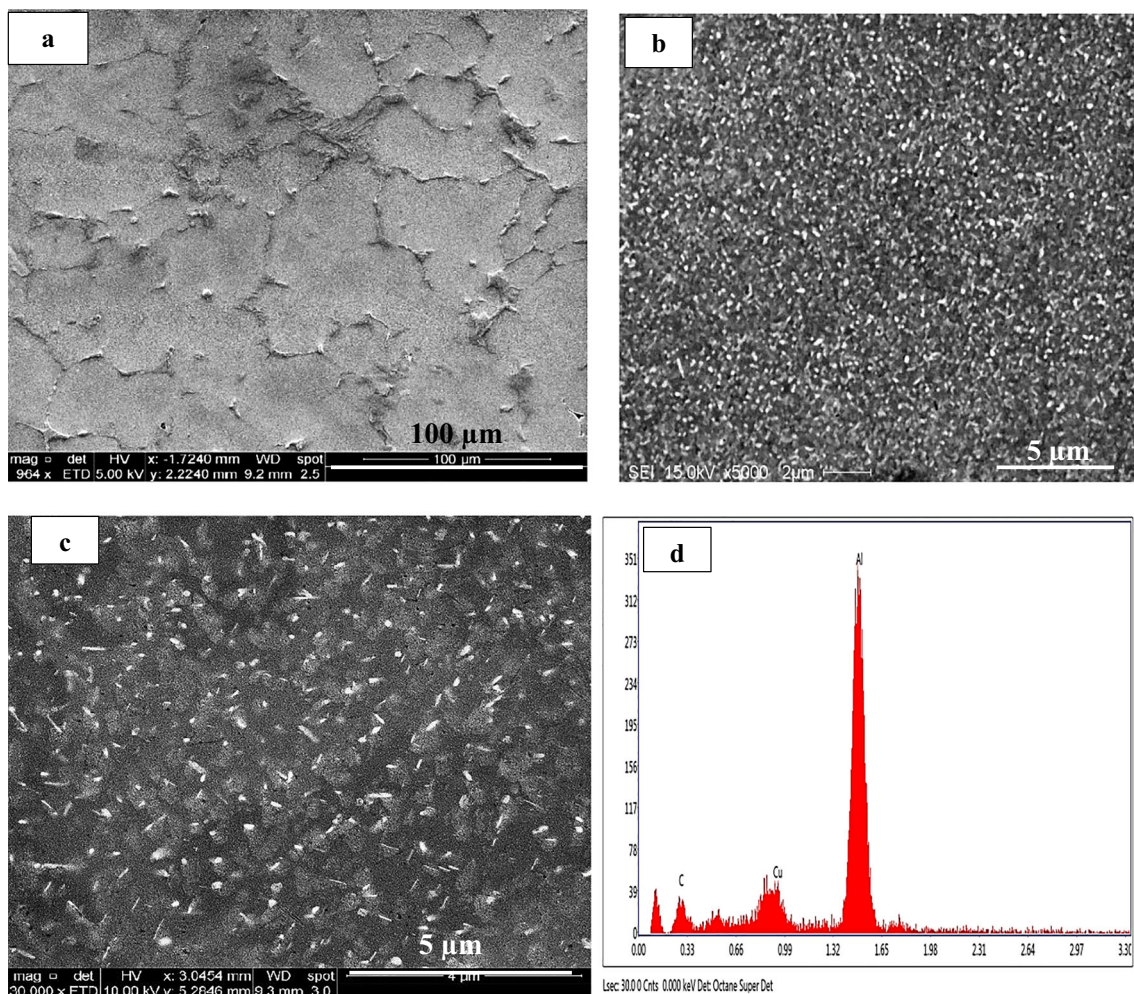
Fig. 5 Backscattered electron images showing precipitation in HT200 alloys: **a** alloy A, **b** alloy B, **c** alloy C, **d** EDS spectrum obtained from **c**
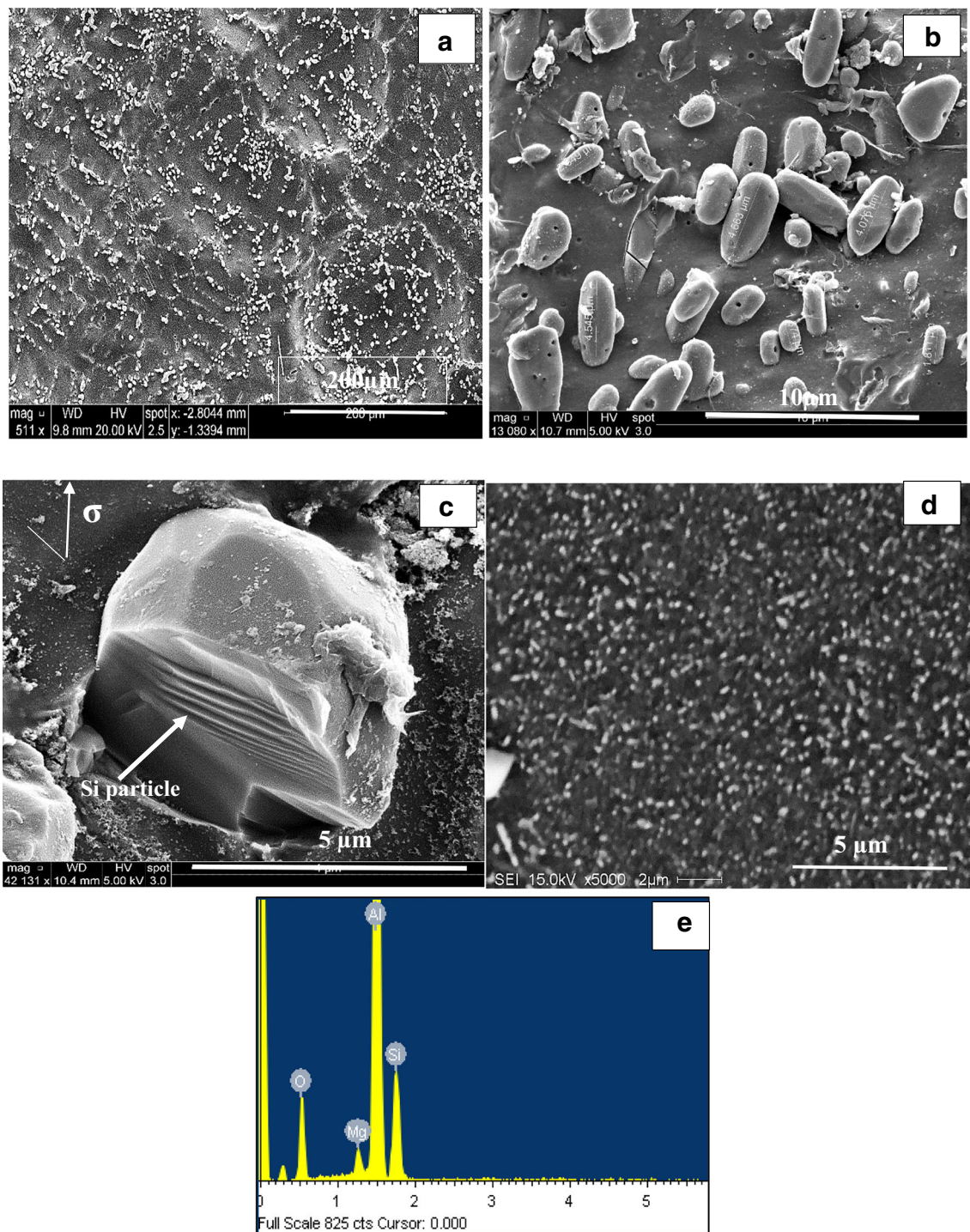
Fig. 6 **a** Backscattered electron image showing precipitation of Si particles following solutionizing treatment, **b** a high-magnification image of **a**-note the marking of the surface of the Si particles, **c** fracture of Si particles under tensile load, **d** ultra-fine Mg_2Si particles in alloy E in the T6 condition, **e** corresponding EDS spectrum

In terms of comparison between alloy HT200 and the commercial alloys, it can be noticed that the T7 heat-treated HT200 alloy (coded alloy C) reveals a comparable performance to the 319 alloy for the T7 treatment in terms of yield strength but with a higher elongation. On the other hand, alloy C exhibits lower yield strength compared to the 356 alloy (T6 heat-treated) despite its comparable ultimate tensile strength and ductility values. Figure 5 demonstrates the effect of heat treatment on the size and distribution of Al_2Cu phase particles in HT200 alloys, as confirmed from the associated EDS spectrum in Fig. 5d. Figure 6 reveals dense precipitation of hard eutectic Si particles in the
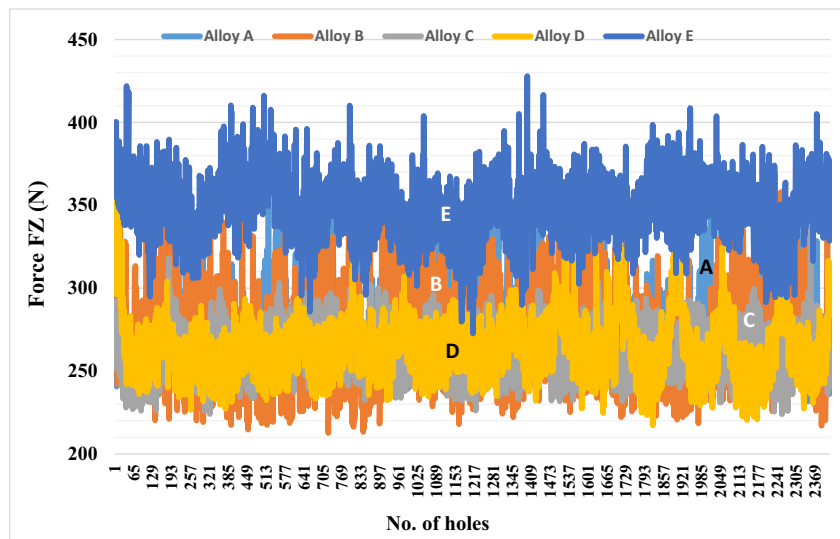
Fig. 7 A schematic diagram showing a drilled block mounted on the drilling stage—180 holes drilled per block (dimensions are in mm)
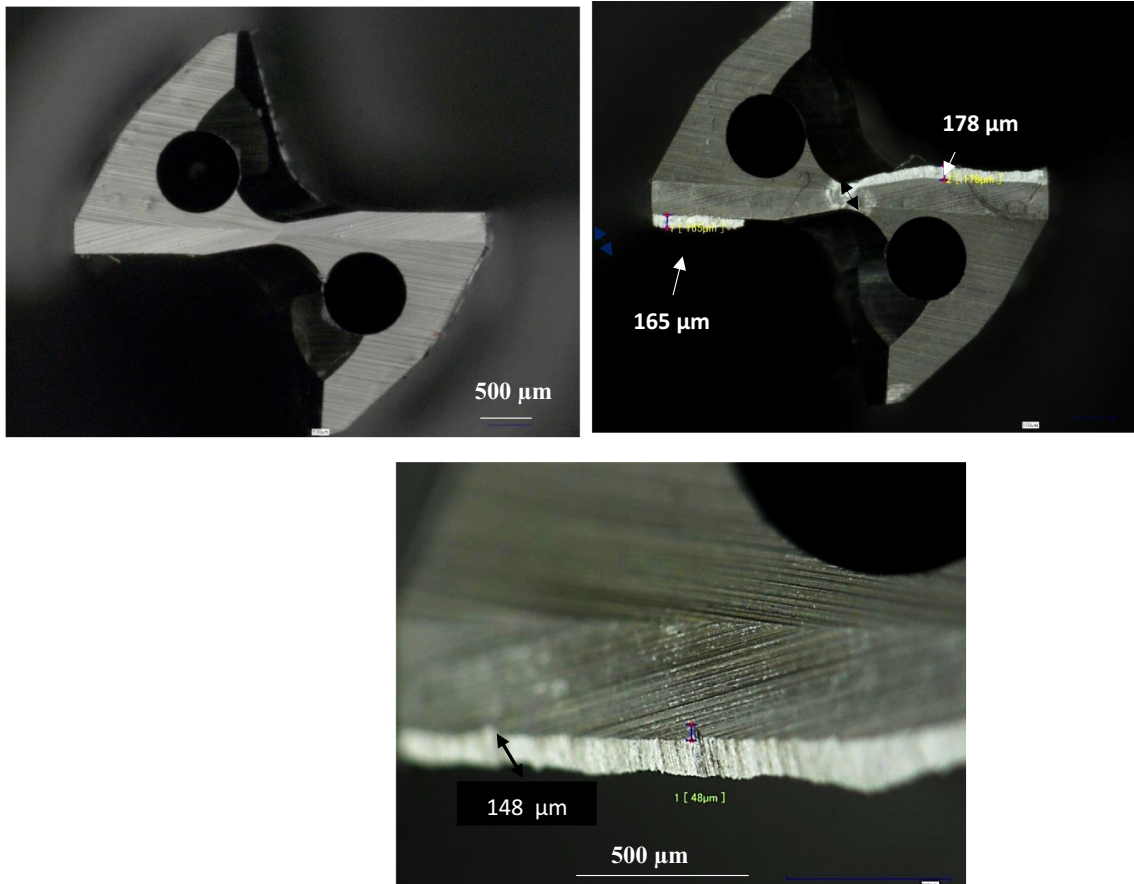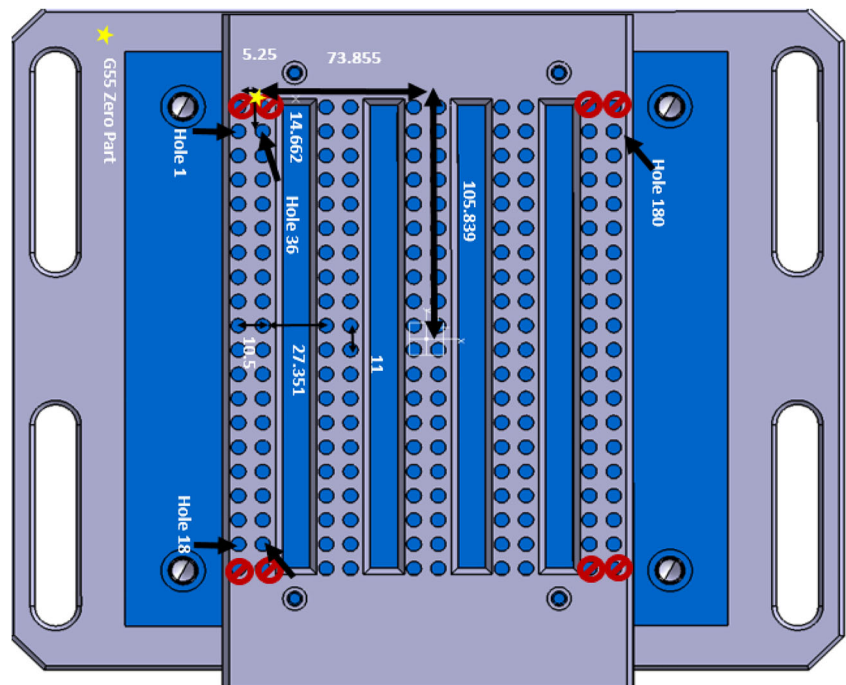
Fig. 8 **a** New drill, **b** same tool after drilling 2700 holes showing signs of wear—alloy A, **c** after 900 holes—alloy E

Fig. 9 Axial cutting forces through different alloys vs number of the drilled holes

matrix during the solidification process (Fig. 6a, 1000 VHN) and Mg$_2$Si phase particles in alloy E in the T6 condition. In a previous study, the authors determined that the Si particle density is approximately 41,500 particles/mm^2 [18]. Considering the cross section area of the drill used (approximately 36 mm^2), the tool is instantaneously passing through ~2 million hard Si particles.

3.2 Drilling characteristics

3.2.1 Cutting forces

A restricted criterion was designed for evaluating tool life for the drilling process. The criterion is to use one tool for each alloy to machine 2700 holes. Three conditions were considered to indicate tool failure: if the full margin width is worn in the outer corner, or flank wear achieves 0.375 mm, or the tool fails or gets broken [6]. Figure 7 shows a schematic presentation of a drilled block whereas

Fig. 8 reveals the wearing of a new tool (Fig. 8a) after drilling 2700 holes (Fig. 8b) using alloys A and E as an example. An important point noted in regard to the cutting tool surface of alloy E (Fig. 8c) was that an initial deterioration and notches appeared on the cutting tool surface with alloy E but not with the HT200 alloys. In alloy E, this notch appears after 900 holes, which indicates fast deterioration of the tool edge, which is to be expected, in keeping with the effect of high silicon content on machinability in the Al-Si alloys.

Initial results for forces were obtained by applying the algorithm methodology over recorded data during the drilling process, as illustrated in Fig. 9. The initial data included 12,500 holes drilled for the five alloys; the data was filtered digitally on 1000 Hz low pass filter to obtain the participating effect of rotation on the axial and resultant force, whereas the rotation frequency is almost 250 Hz. The graph indicates the raw data of axial force and resultant force through 2500 holes for each alloy. Due to the large amount of data in Fig. 9, which

Fig. 10 Average axial cutting forces through different alloys vs number of the drilled block
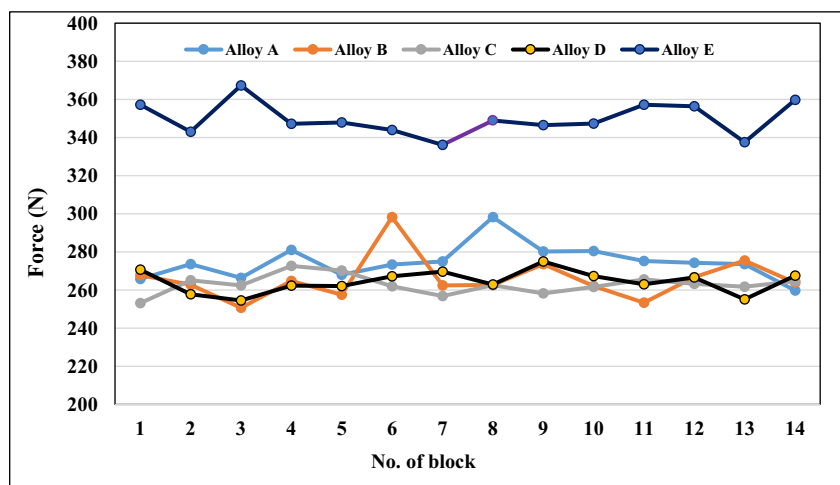
Table 5 Average cutting forces for studied alloys

Alloy	Average Fz (N)*	Average Fr (N)**
Alloy A	276 ± 23	284 ± 27
Alloy B	269 ± 28	276 ± 31
Alloy C	263 ± 15	269 ± 19
Alloy D	265 ± 20	272 ± 22
Alloy E	349 ± 21	354 ± 23

*Drilling direction; **resultant

may mask the actual variation in the drilling forces (Fz), the results were replotted vs number of blocks in Fig. 10, where each spot represents the average of 180 holes drilled per block.

The main observation to be noted from Fig. 10 is that alloy E shows the highest cutting forces in both axial and resultant components, while alloy A shows the minimal cutting forces. In addition, the differences in average cutting forces between alloys B, C, and D are small, although there is a wide difference in their mechanical properties. It can also be noticed that T5 heat treatment of the HT200 alloy, as is the case for alloy B, reduces the necessary cutting forces in the drilling process somewhat, in comparison to the as-cast condition (alloy A). In addition, alloy B performed much better with respect to cutting forces compared to alloy E.

A slight tendency toward increase in the cutting forces with the aging treatment can be noted in the different alloys. This tendency can be noticed by the slight increase in the average force measured for each block for each alloy and may be interpreted in terms of tool deterioration with the number of holes drilled. The average cutting forces are presented in Table 5. These average values were obtained over 180 holes drilled per block × 14 blocks drilled for each alloy.

3.2.2 Built up edge—height and width

BUE is one of the major factors that affect the quality of the machining process, specifically in terms of surface roughness and hardness of the machined surface [20, 21]. Built up edge generally takes place because of heat generated due to friction, as some hardened particles from the flowing metal over the tool surface are welded to the tool edge because of the localized heat to form a new non-regular cutting edge. These chips start to accumulate over the cutting edge until it achieves the critical size to break. Although the mechanism is almost the same for all materials, the built up edges formed in different alloys and cutting conditions vary widely in terms of size and shape [22]. The effect of heat built up edge on the machining process is significant with respect to different variables of the material removal process such as chip size, tool life, surface finish, and dimensional control [10, 15]. In order to control the built up edge building process, various considerations are used in designing the machining process such as increasing the cutting speed and increasing the rake angle of the tool. Oliaei and Karpat [23] reported that the extent of the built up edge and the surface roughness decrease with increasing cutting speed, and that increase in the rake angle decreases side flow and the size of the built up edge.

Figure 11 shows the height of the BUE after taking the measurements through the whole drilling process for the five alloys. As mentioned in the experimental section, coolant showers were used during drilling. Thus, the observed peak in Fig. 11 (alloy B) may have resulted from the soldering of chips as shown in the inset micrograph. Their removal would have taken place because of applied showers of coolant that would have separated the chip from the tool. The BUE over one side did not exceed 543 μm in height—as shown by the broken arrow in Fig. 12b, whereas the highest average was

Fig. 11 Built up height during drilling
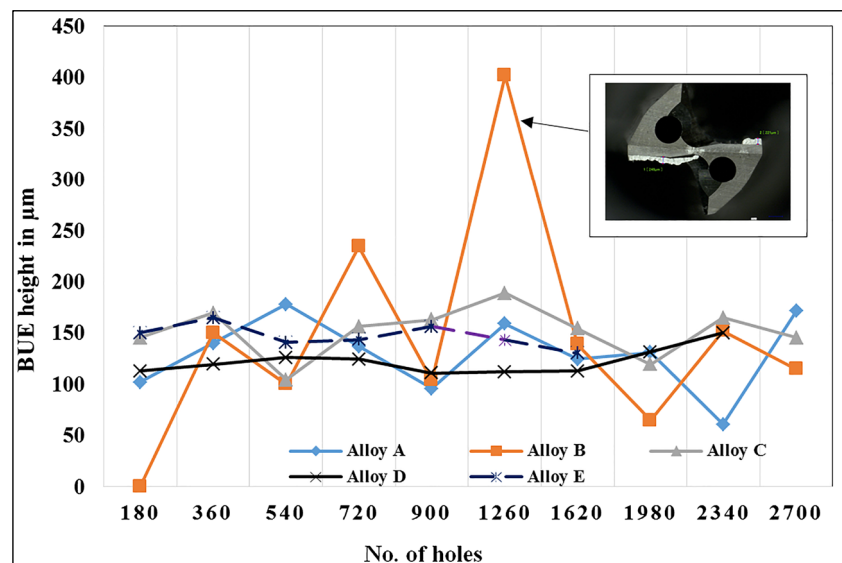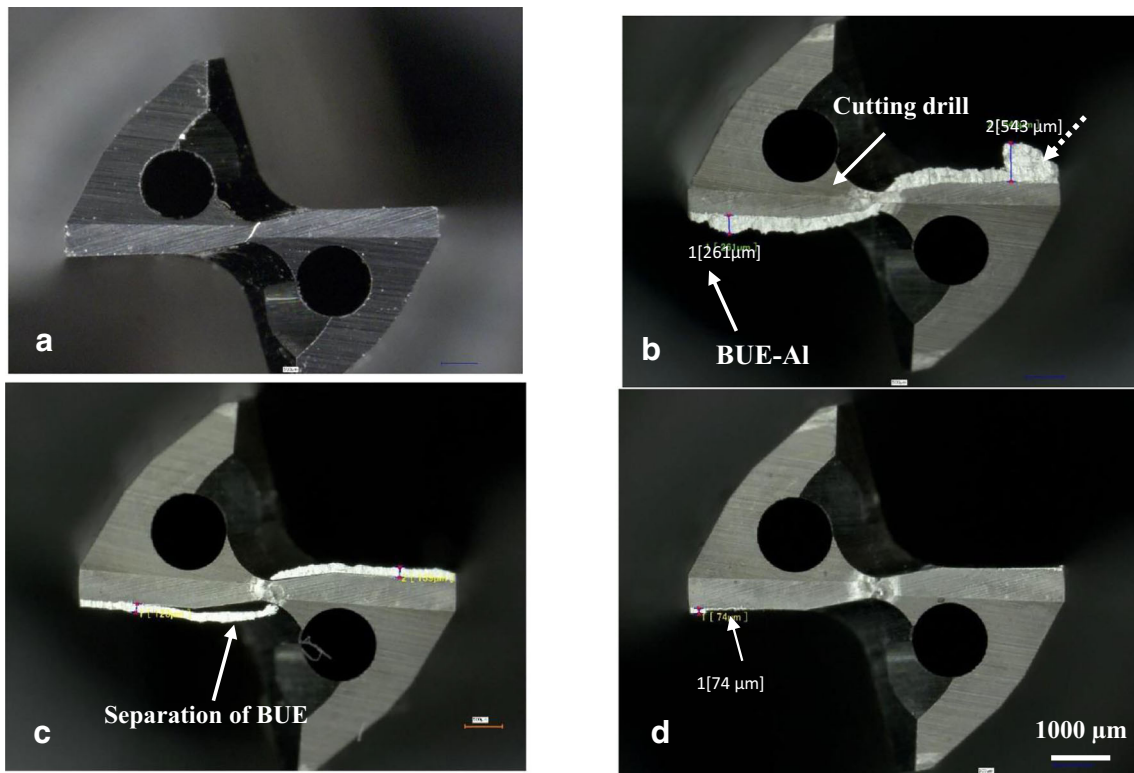
Fig. 12 Changes in the thickness of BUE in with the increase in number of drilled holes: **a** fresh tool, and after **b** 1260 holes (alloy B), **c** 1980 holes (alloy A), **d** 2700 holes (alloy A)

almost 400 μm; both cases were noted for alloy B. In terms of height, alloy B showed a higher tendency to accumulate BUE during drilling, compared to the other alloys, which showed an average BUE within the range of 150 μm. The photograph of the cutting tool in Fig. 12c reveals that separation of BUE starts to occur when its height is around 250 μm on one face. With respect to the built up edge width, it can be noted from Fig. 13 that alloy C had the highest effect on tool BUE accumulation. The average width for alloy C was about 600 μm in comparison to the other alloys with an average of about
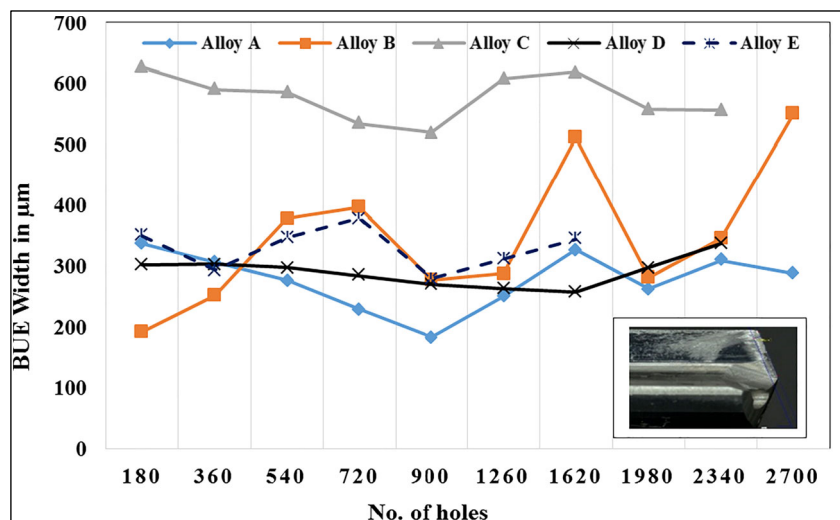
300 μm. Alloy B also showed relatively higher average BUE width measurements than the rest of the alloys, but still lower than alloy C.
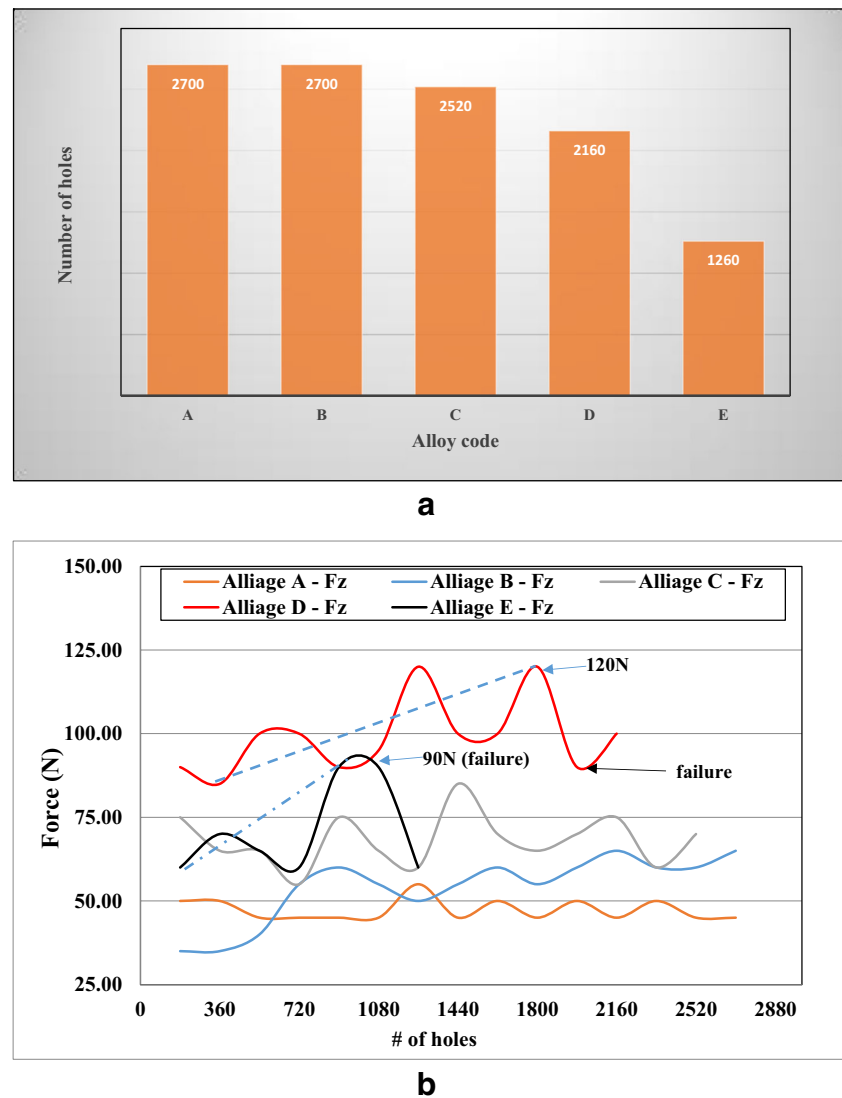
3.3 Tapping characteristics

3.3.1 Tapping forces

Figure 14a and b compare the obtained tapping forces. For similar tapping parameters, alloys D and E generate the

Fig. 13 Built up width in drilling

Fig. 14 Effect of alloy type and heat treatment on **a** number of holes before tool breakage, **b** tapping forces in the Z-direction

a

b

highest cutting forces (~ 120 N) since these alloys have high silicon content (5–7%) compared to tapping forces for the HT200-based alloys (~ 75 N). Note also that for alloy E, the breakage of a tap occurred after 1260 holes, which could indicate that the material is more difficult to machine. A second tapping test was performed to validate this result and it was possible to tap the same number of plates before tool failure. Apparently, the presence of 3.5% Cu in 319 alloy improved the tool life to about 2160 holes, which is approximately half-way between the 356 alloy and alloy A. In other words, the presence of copper in 319 alloy balanced to some extent the tool wearing behavior caused by the eutectic Si particles.

3.3.2 Tap wearing

During the microscope inspection of the tapping tools, no wear could be detected. Figure 15 shows no trace of wear or material transfer presence that could stick on the tools. For this

reason, no graph of wear or accumulation of build-up material could be produced. Figure 15a and b illustrate, respectively, wearing of alloys A and E at the end of the tapping process.

4 Conclusions

Based on the results obtained from this work, the following conclusions may be drawn.

1-   Drilling

   Tool life in drilling tests on Al-Cu alloys regardless the heat treatment can last up to 2700 holes with no sign of failure compared to 900 holes obtained from 356 alloy before wearing. Analysis of the cutting forces showed that alloy E revealed the highest cutting force whereas Al-Cu alloys showed close values. Accumulation of built up

Fig. 15 The state of the tool used to tap the alloy: **a** A, **b** E. Note the absence of wear in **a**
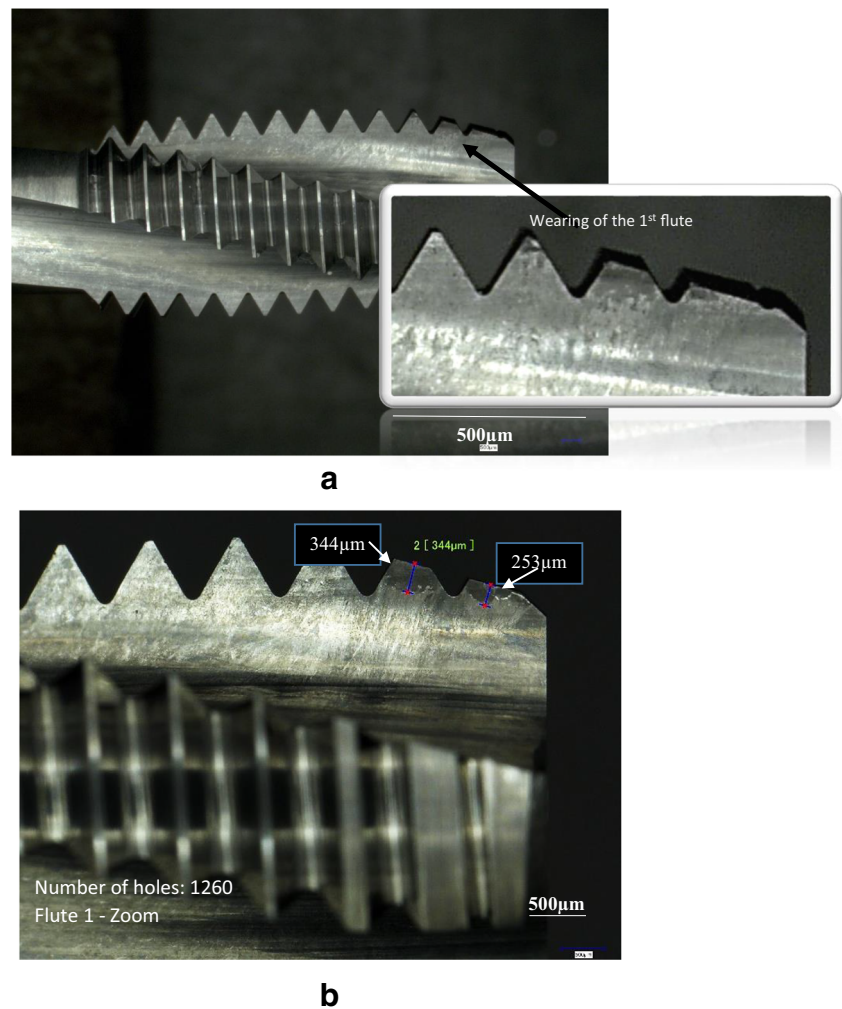
edge showed significant increase in both height and width in alloys B and C, in comparison to alloys A, D, and E. Although all chips had a conical shape, the surfaces of HT200 chips were less shiny compared to those obtained from alloy E.

2- Tapping

The T200-based alloys revealed excellent machinability with no sign of tap wearing after 2700 holes. In contrast, the tool failed after 1600 holes in the case of 356 alloy and after 2160 holes for 319 alloy. Thus, it is concluded that the presence of 3.5% Cu in the 319 alloy may have helped in reducing the severity of wearing due to eutectic Si particles. The tapping forces reached 120 N prior to failure (2160 holes) compared to about 75 N in the case of HT200-based alloys (~ 2700 holes).

References

1. Roy P, Sarangi SK, Ghosh A, Chattopadhyay AK (2009) Machinability study of pure aluminium and Al–12% Si alloys against uncoated and coated carbide inserts. Int J Refract Met Hard Mater 27:535–544

2. Guru PR, Khan F, Panigrahi SK, JanakiRam DG (2015) Enhancing strength, ductility and machinability of an Al–Si cast alloy by friction stir processing. J Manuf Process 18:67–74

3. Pattnaik SK, Bhoi NK, Padhi S, Sarangi SK (2018) Dry machining of aluminum for proper selection of cutting tool: tool performance and tool wear. Int J Adv Manuf Technol 98(1–4):55–65

4. Ye H (2003) An overview of the development of Al-Si-alloy based material for engine applications. J Mater Eng Perform 12:288–297

5. Nur Akmal Hakim Bin Jasni (2013) Cutting performance of advanced multilayer coated (TiAlN/AlCrN) in machining of AISI D2 hardened steel, Master's thesis, Universiti Tun Hussein Onn Malaysia

6. Barzani MM, Sarhan AAD, Farahany S, Singh R, Maher I (2015) Investigating the machinability of Al–Si–Cu cast alloy containing bismuth and antimony using coated carbide insert. Measurement 62:170–178

7. Fang N, Wu Q (2005) The effects of chamfered and honed tool edge geometry in machining of three aluminum alloys. Int J Mach Tools Manuf 45(10):1178–1187

8. Garza Elizondo GH (2010) Machinability of Al-(7-11%)Si casting alloys, M. Eng. Thesis, UQAC, Chicoutimi, Quebec

9. Tash M (2005) Effect of metallurgical parameters on the machining behavior of 356 and 319 alloys (drilling and tapping study), PhD Thesis, UQAC, Chicoutimi, Quebec

10. Garza-Elizondo GH, Samuel E, Mohamed AMA, Samuel AM, Samuel FH, Alkahtani SA (2011) Evaluation of data-processing of drilling forces and moments in aluminum-silicon casting alloys, in 41st International Conference on Computers & Industrial Engineering 2011 Los Angeles, California, USA, 23–25 October 2011. Los Angeles, California. pp. 1081–1086

11. Demir H, Gündüz S (2009) The effects of aging on machinability of 6061 aluminium alloy. Mater Des 30:1480–1483

12. Soares RB, de Jesus AMP, Neto RJL, Chirita B, Rosa PAR, Reis A (2017) Comparison between cemented carbide and PCD tools on machinability of a high silicon aluminum alloy. J Mater Eng Perform 26(9):4638–4657

13. Santos MC Jr, Machado A, Sales WF, Barrozo M, Ezugwu EO (2016) Machining of aluminum alloys: a review. Int J Adv Manuf Technol 86:3067–3080. https://doi.org/10.1007/s00170-016-8431-9

14. Pucella G, Samuel AM, Samuel FH, Doty HW, Valtierra S (1999) Sludge formation in Sr-modified Al-11.5 Wt% Si diecasting alloys. AFS Trans 107:117–125

15. Zedan Y (2010) Machinability aspects of heat-treated Al-(6–11)% Si cast alloys: role of intermetallics and free-cutting elements, PhD Thesis, UQAC, Chicoutimi, Quebec

16. Hamed M (2019) Paramètres de fraisage pour les alliages coulées Al-Cu et Al-Si Cast, M. Eng. Thesis, UQAC, Chicoutimi, Quebec

17. Mohamed AMA, Samuel FH (2012) A review on the heat treatment of Al-Si-Cu/Mg Casting Alloys. In: Heat treatment: conventional and novel applications. p 229

18. Samuel AM, Doty HW, Valtierra S, Samuel FH (2017) New method of eutectic silicon modification in cast Al–Si alloys. Int J Met 11(3):475–493

19. Elsharkawi EA, Abdelaziz MH, Doty HW, Valtierra S, Samuel FH (2018) Effect of β-Al5FeSi and π-Al8Mg3FeSi6 phases on the impact toughness and fractography of Al–Si–Mg-based alloys. Int J Met 12:148–163

20. Sood PK, Sehgal R, Dwived DK (2017) Machinability of hypereutectic cast Al–Si alloys processed by SSM processing technique. Sadhana 42:365–378

21. Uhlmanna E, Flögela K, Sammlera F, Riecka I, Dethlefsa A (2014) Machining of hypereutectic aluminum silicon alloys, 6th CIRP International Conference on High Performance Cutting, vol. 14, pp. 223–228

22. Ahmed YS, Fox-Rabinovich G, Paiva JM, Wagg T, Veldhuis SC (2017) Effect of built-up edge formation during stable state of wear in AISI 304 stainless steel on machining performance and surface integrity of the machined part. Materials 10:1230. https://doi.org/10.3390/ma10111230

23. Oliaei SNB, Karpat Y (2016) Investigating the influence of built-up edge on forces and surface roughness in micro scale orthogonal machining of titanium alloy Ti6Al4V. J Mater Process Technol 235:28–40